Effects of postdeposition annealing on the structure and optical properties of YO_xN_y films

X. J. Wang,[a] L. D. Zhang,[b] G. He, J. P. Zhang, M. Liu, and L. Q. Zhu
Key Laboratory of Materials Physics, Anhui Key Laboratory of Nanomaterials and Nanostructure, Institute of Solid State Physics, Chinese Academy of Sciences, Hefei 230031, China

(Received 6 September 2007; accepted 5 January 2008; published online 17 March 2008)

High-k gate dielectric YO_xN_y films were prepared by reactive sputtering. The effects of postdeposition annealing on the structure and optical properties of YO_xN_y films have been investigated. The x-ray diffraction result shows that the crystallization starts at the annealing temperature of 500 °C. Spectroscopic ellipsometry was employed to determine the optical properties of a set of YO_xN_y films annealed at various temperatures. It was found that the refractive index (n) of YO_xN_y films decreased with the increase of annealing temperature below 600 °C, whereas it increased with increasing annealing temperature above 600 °C. The annealing-temperature dependence of the optical band gap of YO_xN_y films was also discussed in detail. It has indicated that the optical band gap of YO_xN_y films shifts to higher energy after higher temperature annealing, which is likely due to the reduction of N content and the change of crystalline structure in YO_xN_y films. © *2008 American Institute of Physics*.
[DOI: 10.1063/1.2890987]

I. INTRODUCTION

Beyond the 70 nm node for scaled silicon complementary metal oxide semiconductor (CMOS), the exponential increase in leakage current for SiO_2 and SiO_xN_y with decreasing thickness will prohibit the use of these materials as gate dielectrics in future generations of advanced devices. As a result, a high-k gate dielectric material is needed to replace the traditional SiO_2 and SiO_xN_y.[1] Among many high-k gate dielectric materials such as Ta_2O_5, TiO_2, ZrO_2, and HfO_2, Y_2O_3 has been considered to be one of the most promising candidates because of high dielectric constant (k) up to 18, potential thermodynamic stability in contact with Si, and high conduction band offset with silicon (~2.3 eV).[2–4] In addition, it has shown promising results in terms of leakage current, equivalent oxide thickness.[5] Moreover, high effective mobilities in yttrium oxide based n-channel metal oxide semiconductor field-effect transistors with values of 210 $cm^2 V/s$ have been reported.[6] However, the use of all the metal oxide and silicate films on Si including Y_2O_3 as high-k gate dielectric replacement for silicon dioxide and oxynitride in advanced ultralarge scale integration technologies presents several difficulties. Some of the key topics concerned are density of interface states, reliability, chemical, and structural stability, oxidation of the Si substrate, diffusion of metallic species into the active semiconductor region, and transport of Si into the high-k film.[7,8] The incorporation of nitrogen into the high-k gate dielectric film or at the high-k gate dielectric interface with the Si substrate could be advantageous in overcoming the above-mentioned difficulties. It has been found that the incorporation of nitrogen into the high-k gate dielectric film would be effective in suppressing oxygen diffusion and impurity penetration through high-k oxides,[9,10] inhibiting interfacial reaction with the Si substrate,[11] increasing crystallization temperature,[12] and improving the electrical performance of the device.[13,14]

Nitrogen incorporation technology has been extensively studied in SiO_2 gate dielectric films. Typically, high temperature annealing of SiO_2 in N_2O, NO, or NH_3 gas ambients results in a high nitrogen concentration in SiO_2 film or at the SiO_2/Si interface. It has been shown that incorporation of nitrogen in SiO_2 gate dielectric films is beneficial in Si-based microelectronic devices and model device systems.[15] Nitrogen incorporation technology has also been extensively investigated in high-k gate dielectric field recently, such as AlO_xN_y, ZrO_xN_y, HfO_xN_y, and $HfSiO_xN_y$.[16–19] However, there have been few reports on the optical properties of the nitrogen-incorporated Y_2O_3 films.

Spectroscopic ellipsometry (SE) is known as a sensitive and nondestructive method for thin film characterization. It has been reported that sensitive change in the dielectric functions in SE data can provide information on crystallization and densification of the film during the annealing treatment.[20] Moreover, the spectral modification also reflects the change in the chemical bonding state because the reformation in bond type caused by structural changes can modify the shape of the spectrum in the refractive index and extinction coefficient.[21]

In this work, we fabricated nitrogen-incorporated Y_2O_3 gate dielectrics by reactive sputtering. The surface topography of the YO_xN_y films annealed at different temperatures was examined by atomic force microscopy (AFM). The structures of YO_xN_y were investigated by x-ray diffraction (XRD) with Cu $K\alpha$ radiation, and the surface chemical states were examined by x-ray photoelectron spectroscopy (XPS).

Spectroscopic ellipsometry was used to investigate the optical characteristics of YO_xN_y films in relation to anneal-

[a]Electronic mail: xjwang2007@yahoo.com.cn.
[b]Author to whom correspondence should be addressed. Electronic mail: ldzhang@issp.ac.cn.

 © 2008 American Institute of Physics

Downloaded 21 Jun 2010 to 61.190.88.137. Redistribution subject to AIP license or copyright; see http://jap.aip.org/jap/copyright.jsp

ing temperature. The change of refractive index and extinction coefficient of the YO_xN_y films upon high temperature annealing has been demonstrated. The dielectric functions and optical band gap change of the YO_xN_y films at various annealing temperatures has also been discussed.

II. EXPERIMENT

The YO_xN_y films were deposited by reactive sputtering of Y target with purity of 99.99% in $Ar+N_2$ ambient $[N_2/(Ar+N_2)=0.25]$. The sputtering chamber was evacuated to 9.6×10^{-4} Pa before Ar and N_2 gases were introduced. The films were deposited onto *n*-type Si (100) single crystal substrates with resistivity of 4–12 Ω cm. Prior to deposition, the Si substrate was cleaned by Radio Corporation of America (RCA) cleaning, followed by etching in 100:1 diluted HF solution, resulting in a hydrogen terminated surface. During deposition, the substrate temperature and total working pressure were maintained at approximately 100 °C and 0.8 Pa, while the rf power and substrate-to-target distance were kept at 100 W and 5.5 cm, respectively. As well known, yttrium has a very high affinity for oxygen, thus the as-deposited film was expected to be YO_xN_y due to the existence of residual oxygen in the system, the atomic concentration of nitrogen in the as-deposited film is 7.52 at. % as determined by XPS. In order to investigate the annealing-temperature dependence of optical properties for YO_xN_y films, the as-prepared YO_xN_y films were then subjected to a postdeposition annealing in O_2 ambient at different temperatures ranging from 300 to 800 °C for 10 min.

Film structure was analyzed by XRD (Bruker D8, Germany) with a Cu $K\alpha$ beam under an accelerated voltage of 40 kV and a current of 30 mA at a scan rate of 3/min. The interfacial property was investigated by Fourier transform infrared spectroscopy (FTIR) in transmission mode.

A Digital Instrument (DI) 3100 AFM was employed to study the surface morphology of the YO_xN_y films annealed at different temperatures. The typical scan range varied between 1 and 10 μm. The vertical sensitivity is better than 0.1 nm. XPS was used to analyze the composition of the films.

An *ex situ* phase modulated spectroscopic ellipsometry (UVISEL Jobin–Yvon) was used to investigate the optical properties of the YO_xN_y films at different annealing temperatures in the spectral range of 1.5–6.5 eV with a step of 50 meV at an incident angle of 70°. Spectroscopic ellipsometry measures the changes in polarization state between incident and reflected light on the samples. The transformation of polarization is the result of different phenomena such as interferences due to the thin film structure of the sample, optical properties of the medium, and interface. The standard experimental quantities measured by the spectroscopic ellipsometry are the angle ψ and Δ, which are related to the optical and structure properties of the samples, and defined by

$$\rho = r_p/r_s = \tan \psi e^{i\Delta},$$

where r_p and r_s are the complex reflection coefficients of the light polarized parallel and perpendicular to the plane of the incidence, respectively. The measured ellipsometric spectra are then fitted with an appropriate fitting model, which is constructed on the basis of the sample structure. The thickness and the optical constants, i.e., the refractive index and extinction coefficient, of the films were calculated on the basis of the best fit between the experimental and simulated spectra. All fits used the reduced χ^2 as the figure of merit of the fitted function.

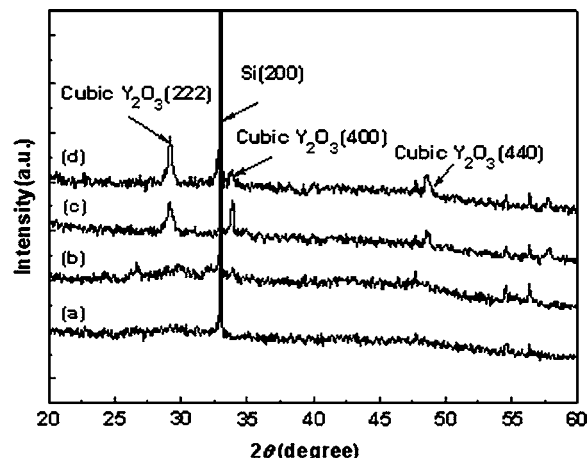

FIG. 1. XRD pattern for YO_xN_y films annealed at different temperatures: (a) 300 °C, (b) 500 °C, (c) 600 °C, (d) and 700 °C.

III. RESULTS AND DISCUSSION

A. Structural characterization

Figure 1 shows the XRD results on YO_xN_y thin films as a function of postdeposition annealing in the range between 300 and 700 °C. The result shows that the crystallization just starts when the annealing temperature reaches 500 °C. For films annealed at lower annealing temperatures, the XRD does not exhibit any peaks and the films are still in amorphous form. For higher annealing temperature, typical diffraction peaks of cubic Y_2O_3 crystal appear. As the annealing temperature increases, the intensity of (222) peak increase, whereas the intensity of (400) peak decrease, which indicates that the (222) plane is the preferential orientation during the nanocrystal growth process. The mean size of the nanocrystallties was deduced from the well-known Scherrer's formula,[22] i.e.,

$$B(2\theta) = 0.9\lambda/L \cos \theta,$$

where $B(2\theta)$ is the full width at half maximum (FWHM) of the most intensity peak in the XRD pattern. The value of λ is 0.154 nm. From the (222) peaks, the nanocrystal sizes are 7 and 10 nm for samples annealed at 600 and 700 °C, respeatively. By calculation, it is concluded that the size of nanocrystally increases with increasing annealing temperature.

Surface uniformity becomes crucial for oxide reliability issues when the thickness of the high-*k* gate dielectric is several nanometers. Figure 2 shows the three-dimensional AFM images of the YO_xN_y films annealed at different temperatures. It was found that the roughness root mean square (rms) value increased with the increase of annealing temperature, with approximately 0.53, 1.02, 1.12, and 1.56 for

Downloaded 21 Jun 2010 to 61.190.88.137. Redistribution subject to AIP license or copyright; see http://jap.aip.org/jap/copyright.jsp

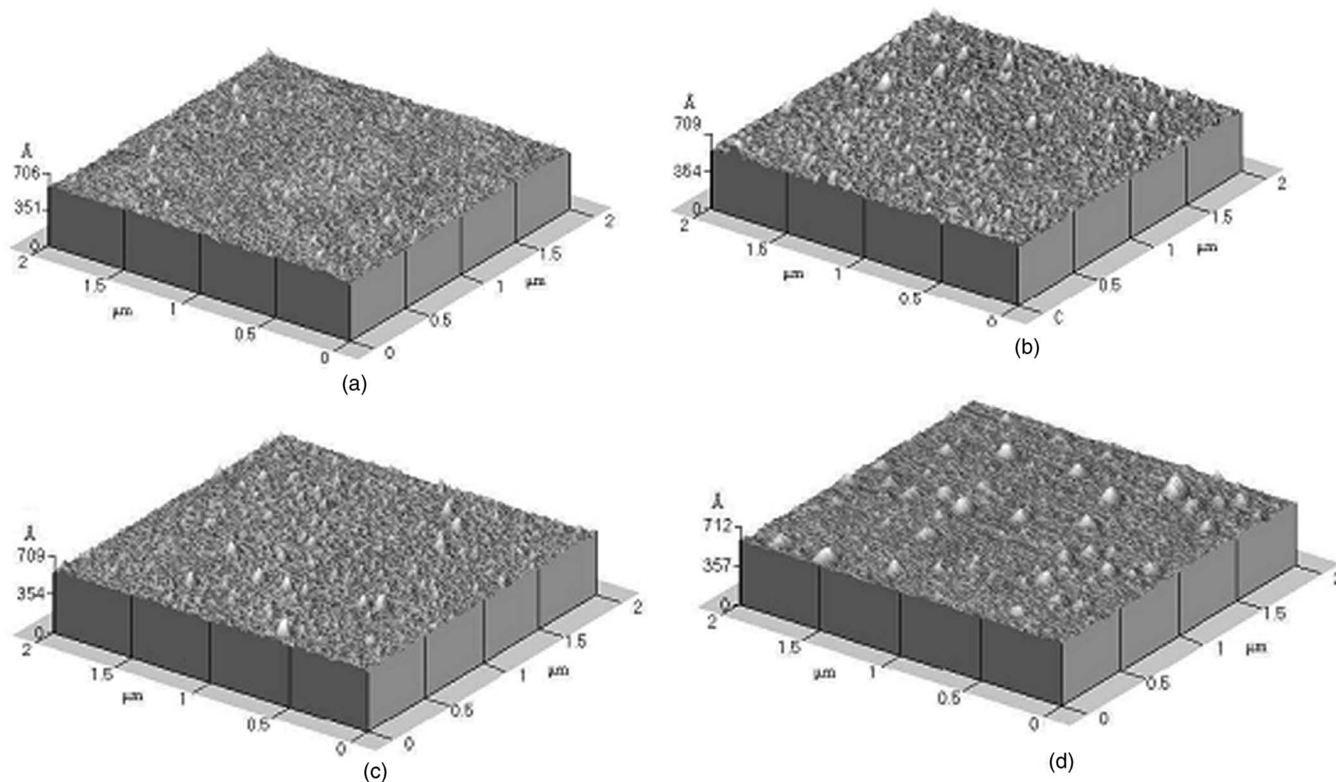

FIG. 2. Three-dimensional AFM images of YO_xN_y thin films annealed at different temperatures of (a) 300 °C, (b) 500 °C, (c) 600 °C, (d) 800 °C, respectively. All the images display 2×2 μm scan.

YO_xN_y films annealed at 300, 500, 600, and 800 °C, respectively. The increase of the roughness of YO_xN_y film surface with increasing annealing temperature is likely due to crystallization-induced large grain size, as indicated by XRD results.

B. Chemical bond states of the films

Figure 3 shows XPS spectra for YO_xN_y films annealed at different temperatures. The Y3*d* spectrum in Fig. 3(a) shows a doublet due to spin-orbit splitting into the Y3*d*3/2 and Y3*d*5/2 components at 158.8 and 156.8 eV, respectively. The area of Y3*d*5/2 peaks increases as the substrate temperature increases. This indicates that, as the annealing temperature increases, the YO_xN_y films have more oxygen content.[23] The O1*s* spectrum in Fig. 3(b) consists of the main peak of O^{2-} bonded to Y^{3+} with a lower binding energy of 529.5 eV and subpeaks such as physisorbed O_2 or hydrated O species with a higher binding state of over 530.0 eV. The areas of the peaks formed by O^{2-} bonded to Y^{3+} increase as the annealing temperature increases, while those of the subpeaks decrease. This indicates that the quantity of oxygen bonding with yttrium in the YO_xN_y film increases as the temperature increases. The XPS result shows that the ratio of O:Y for YO_xN_y films annealed at 300, 500, and 800 °C is 1.416, 1.472, and 1.497, respectively. Therefore, it is likely that higher annealing temperature results in less oxygen vacancies.

Figure 3(c) shows the XPS spectra for N1*s* core level of the YO_xN_y film annealed at temperatures of 300, 500, and 800 °C, respectively. N1*s* photoemission spectra are normalized at the peak-height maxima with curve-fitting results. For all the annealed samples, the deconvoluted spectra of N1*s* shows two components associating with two chemical states. One of them, at a binding energy E_b=404.2 eV, corresponding to N–O bond (N1),[18] whereas the other, at E_b =407.9 eV, is attributed to the N atom in a $N\equiv O_3$ configuration surrounded by three O atoms,[24] hereafter called $N\equiv O_3$ bonds (N2). As shown in Fig. 3(c), there is no significant change of the peak corresponding to N–O bond with annealing temperature, indicating the stability of N–O bond upon high temperature annealing. However, the intensity of the peak corresponding to $N\equiv O_3$ bonds has a constant decrease with increasing annealing temperature, indicating the thermal instability of $N\equiv O_3$ bonds upon high temperature annealing. After the film annealed at 800 °C, $N\equiv O_3$ bonds almost disappear. Using standard sensitivity factors for O1*s*, N1*s*, and Y3*d*, the average nitrogen composition is determined to be 3.68, 2.95, and 1.86 at. % for the YO_xN_y films annealed at 300, 500, and 800 °C, respectively.

C. Optical properties

We adopt the Tauc–Lorentz (TL) dispersion function[25] to characterize the dielectric functions of the YO_xN_y films. Essentially, the imaginary part (ε_2) of dielectric functions is obtained by combining the classical expression of the imaginary part of the dielectric functions above the band edge and the standard Lorentz expression, and the real part (ε_1) of dielectric functions is the result of self-consistent Kramers–Kronig integration of ε_2. The following equations summarize ε_1 and ε_2 as a function of photon energy E:

Downloaded 21 Jun 2010 to 61.190.88.137. Redistribution subject to AIP license or copyright; see http://jap.aip.org/jap/copyright.jsp

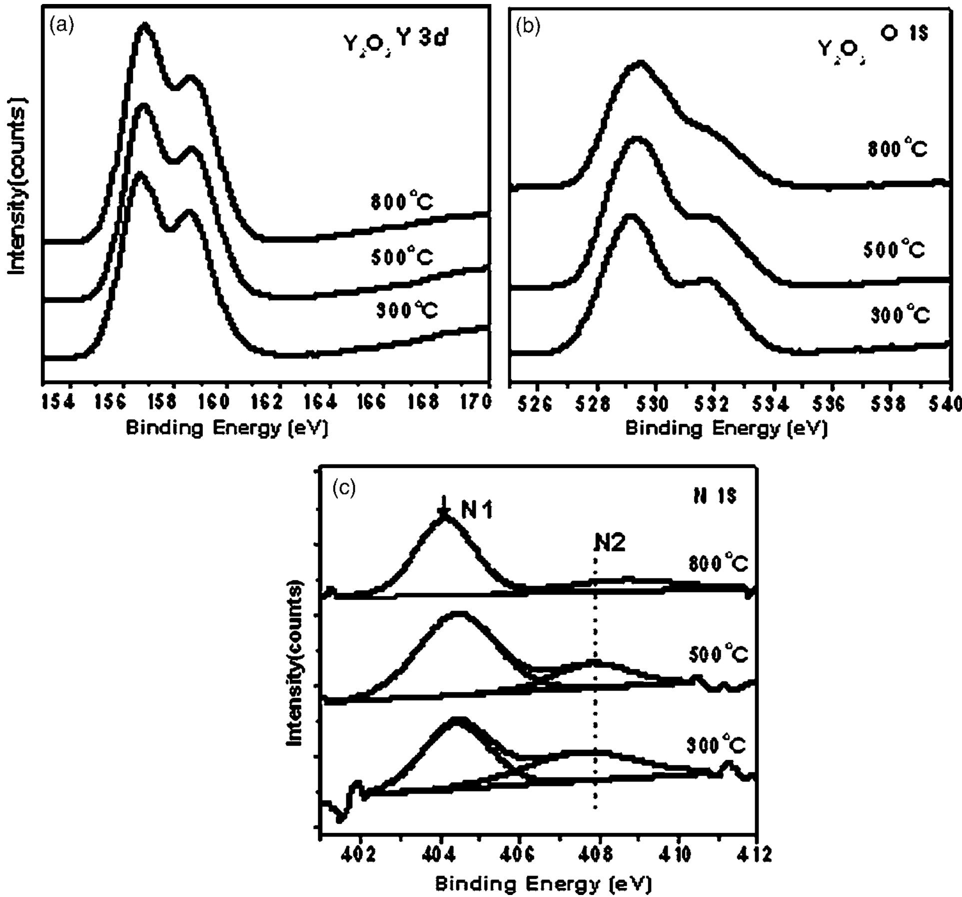

FIG. 3. XPS spectra of YO_xN_y films annealed at different temperatures. (a) Y3*d* core level spectra. (b) O1*s* core level spectra. (c) N1*s* core level spectra.

$$\varepsilon 1(E) = \begin{cases} \dfrac{AE_0C(E-E_g)^2}{(E^2-E_0^2)^2+C^2E^2}\cdot\dfrac{1}{E} & (E > E_g) \\ 0, & (E \leq E_g), \end{cases} \quad (1)$$

and

$$\varepsilon 2(E) = \varepsilon_\infty + \frac{2}{\pi}P\int_{E_g}^{\infty}\frac{\xi\varepsilon_2(\xi)}{\xi^2-E^2}d\xi. \quad (2)$$

Equations (1) and (2) are uniquely defined by five parameters ε_∞ A (transition matrix element), C (broadening term), E_0 (peak transition energy), and E_g (optical band gap).

The ellipsometric delta data is very sensitive to surface quality, therefore, it is very important to include surface roughness in all ellipsometric models to avoid nonphysical absorption artifacts in the optical constants. The roughness was modeled as a mixture of 50% void and 50% bulk material using a Bruggeman effective medium approximation (BEMA).[26] On the other hand, our FTIR result (Fig. 4) has shown that no interfacial layer formed between YO_xN_y films and Si substrate when the film is annealed at temperatures below 600 °C, whereas a perceptible peak associating with the asymmetrical stretching Si–O–Si mode of SiO_2 was found for the film annealed at 600 °C, indicating the growth of interfacial SiO_2 layer between YO_xN_y film and Si substrate. Based on the reasons mentioned above, we used the simple ellipsometric three-phase optical model consisting of the silicon substrate/YO_xN_y film/YO_xN_y film with voids to represent the films annealed at temperatures below 600 °C, while four-phase model consisting of substrate/interfacial layer/YO_xN_y film/YO_xN_y film with voids was adopted to represent the films annealed at temperatures above 600 °C, as shown in Fig. 5. For each sample, the five TL parameters

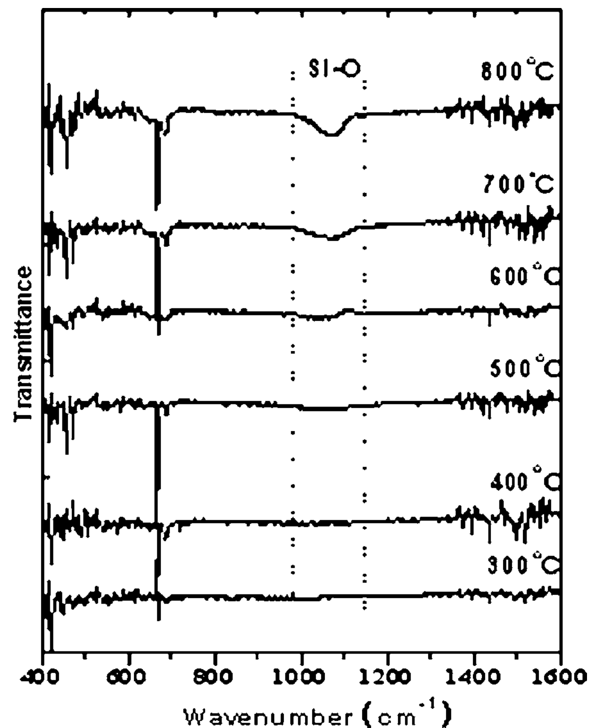

FIG. 4. The annealing-temperature dependence of dielectric functions of YO_xN_y films. (a) The real (ε_1) part of dielectric functions. (b) The imaginary (ε_2) part of dielectric functions.

Downloaded 21 Jun 2010 to 61.190.88.137. Redistribution subject to AIP license or copyright; see http://jap.aip.org/jap/copyright.jsp

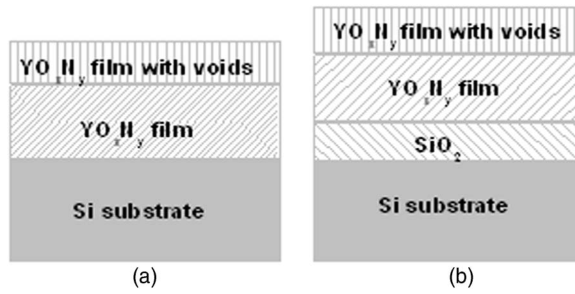

FIG. 5. Schematic representation of the models used for optical simulations. (a) three-phase optical model. (b) four-phase optical model.

and the film thickness are determined by least-squares fitting of their experimental data. However, for ultrathin layers, the accurate determination of each fitting parameter is a difficult matter because of the correlation among them. In order to get high accuracy, the thickness of the surface rough layer (sr) is set at a certain value from the AFM analysis. The surface rough layer thickness is listed in Table I, which is double the AFM root mean square (rms) values based on the reports of Song *et al.*[27] Table I lists all the TL parameters along with the fitting residual χ^2, which represents the goodness of fitting. Shown in Fig. 6 are both the experimental (open circles) and fitted (solid lines) date of YO_xN_y films annealed at 300, 600, and 800 °C, respectively. Spectra represents the I_c and I_s quantities which are given by $I_c = \sin 2\psi \cos \Delta$ and $I_s = \sin 2\psi \sin \Delta$. It is clearly seen that the fit data reproduce almost identically the experimental data in the full spectral range that measured from 1.5 to 6.3 eV.

Figures 7(a) and 7(b) present the annealing temperature dependence of refractive index (n) and extinction coefficient (k) of the YO_xN_y films as a function of photon energy. In Fig. 7(a), it can be seen that the refractive index (n) of the YO_xN_y film annealed at 300 °C is higher than that of the film annealed at 600 °C, whereas the refractive index (n) of the film annealed at 600 °C is lower than that of the film annealed at 800 °C. We have also investigated the refractive index (n) of the films annealed at temperature of 400, 500, and 700 °C, respectively (not shown here), and found that the refractive index (n) of YO_xN_y films decreased with the increase of annealing temperature below 600 °C, while it increased with increasing annealing temperature above 600 °C. It has been reported that increasing the content of nitrogen incorporation in the nitrided oxide films lead to the increase of refractive index (n) due to the fact that metal-nitrogen bonds tend to be less polar than the corresponding metal-oxygen bonds.[28] Our XPS studies of N1s core level spectral have shown that the content of nitrogen reduced with the increase of annealing temperature, thus the decrease

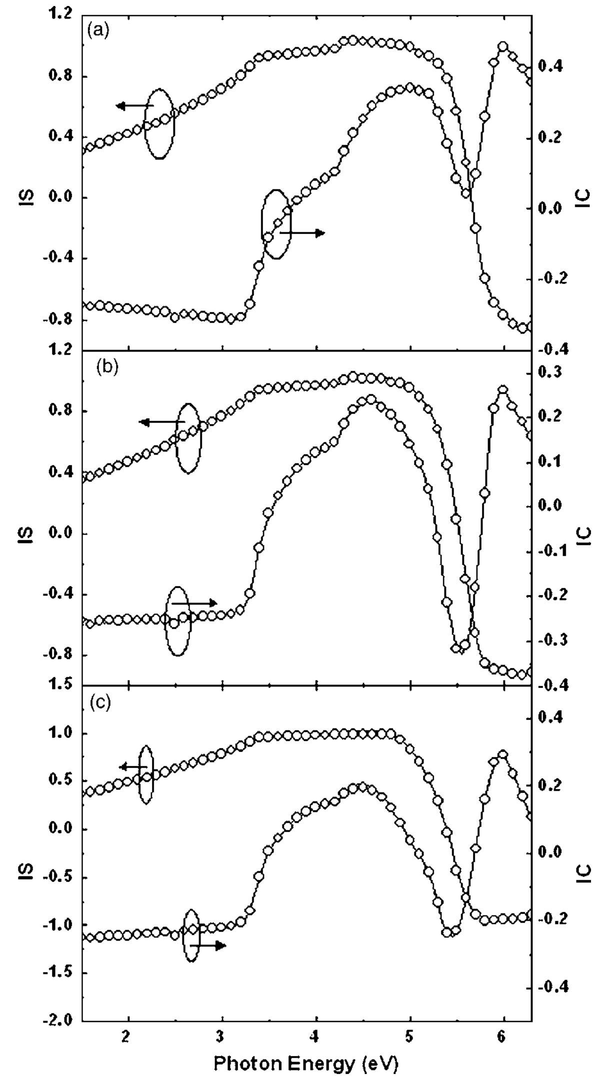

FIG. 6. Experimental (open circles) and fitted (solid lines) spectroscopic ellipsometric data I_s and I_c for YO_xN_y films annealed at different temperatures: (a) 300 °C, (b) 600 °C, and (c) 800 °C.

of refractive index with the increase of annealing temperature below 600 °C is likely due to the reduction of nitrogen content in the YO_xN_y films. On the other hand, the increasing packing density would also lead to a higher refractive index as reported by Hu *et al.*[29] As for the film annealed at temperature above 600 °C, the content of nitrogen is very low, while the packing density is increased due to the fact that higher temperature annealing increases the mobility of the atoms or molecules in the film, which results in the formation of more closely packed thin films. As a result, the increase of packing density leads to the increase of refractive

TABLE I. Parameter values of the fitting results from all samples using TL model dispersion.

Annealing temperature (°C)	t (nm)	A	E_g (eV)	E_0 (eV)	C	ε_∞	AFM rms (nm)	SE sr(nm)	χ^2
300 °C	27.24 ± 0.41	126.19 ± 14.31	5.05 ± 0.05	7.29 ± 0.11	2.82 ± 0.34	1.46 ± 0.22	0.53	1.06	1.22
600 °C	27.46 ± 0.45	140.32 ± 12.18	5.36 ± 0.03	6.73 ± 0.20	4.93 ± 0.28	1.22 ± 0.08	1.12	2.44	2.21
800 °C	27.97 ± 0.32	186.32 ± 34.96	5.72 ± 0.14	7.25 ± 0.15	2.96 ± 0.14	1.02 ± 0.12	1.56	3.12	2.53

Downloaded 21 Jun 2010 to 61.190.88.137. Redistribution subject to AIP license or copyright; see http://jap.aip.org/jap/copyright.jsp

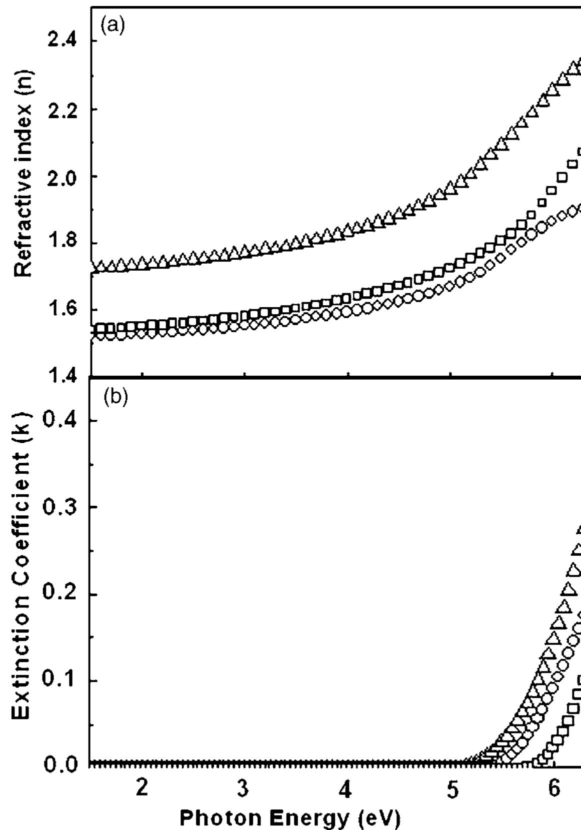

FIG. 7. The annealing-temperature dependence of refractive index (n) and extinction coefficient (k) of YO_xN_y films. (a) The refractive index (n) of YO_xN_y films. (b) Extinction coefficient (k) of YO_xN_y films.

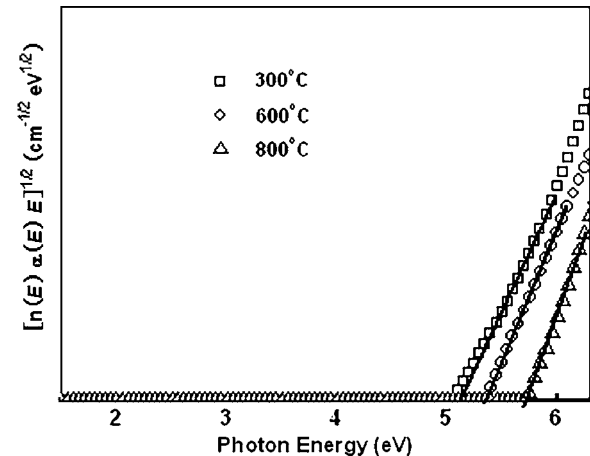

FIG. 8. Tauc plots for determining the optical band gap E_g which is the intercept of the linear fitting curve extrapolated to the zero absorption for YO_xN_y films annealed at temperature 300, 600, and 800 °C, respectively.

index of YO_xN_y films when annealed at temperature above 600 °C. As shown in Fig. 7(b), the extinction coefficient of the YO_xN_y films decreases with the increase of annealing temperature. It can be explained that, for the YO_xN_y film annealed at low temperatures, there exist a large amount of defects, after higher temperature annealing in oxygen ambient, the defects decrease and the films are fully oxidized, and thus lead to the good quality of YO_xN_y films, as shown in our XPS result.

Another parameter that will be discussed is the optical band gap (E_g) derived from the inverted dielectric functions. Even though Eg's were obtained from fitting the data to the TL model, they are not accurate due to the correlation between the fitting parameters.[30] Generally, the band gap for an amorphous material is determined from the energy dependence of its absorption coefficient, $\alpha=4\pi k/\lambda$, near its absorption edge, where λ is the photon wavelength and k is the extinction coefficient which can be calculated from ε_1 and ε_2 by the complex relation $(n+ik)^2=(\varepsilon_1+i\varepsilon_2)^2$ with n being the index of refraction. The most commonly used method to acquire E_g is to use the Tauc plot. Tauc and co-workers showed that near the absorption edge of some amorphous materials, the expression $[n(E)\alpha(E)E]^{1/2}$ varies linearly with $(E-E_g)$ where E is the photon energy. If a straight line is obtained near the band edge in a plot of $[n(E)\alpha(E)E]^{1/2}$ versus the photon energy E, then the extrapolation to zero absorption results in the value of E_g.[30] Figure 8 presents the Tauc plots as illustrated by the $[n(E)\alpha(E)E]^{1/2}$ versus photon energy (E). The bandgap values extracted by extrapolating the straight line near the band edge to zero are 5.09, 5.37, and 5.74 eV for the YO_xN_y films annealed at 300, 600, and 800 °C, respectively. It is clear that the optical band gap increases with the increase of annealing temperature. The change of optical band gap with the annealing temperature is likely due to two factors. Shang *et al.*[31] have found that the incorporation of nitrogen into high-k gate oxides leads to the band gap narrowing by mixing N2p states with O2p states. Our XPS result has shown that the content of nitrogen in YO_xN_y films reduced with the increase of annealing temperature, thus the reduction of nitrogen in YO_xN_y films upon high temperature annealing would lead to the blueshift of band gap. On the other hand, the crystalline structure also has a large effect on the band gap of oxides. Sayan *et al.*[32] have observed that crystalline oxides may have larger band gap. Our XRD result has shown that the crystallization starts at the annealing temperature of 500 °C, and with the increase of annealing temperature, the crystalline degree is increased. Therefore, the change of the crystalline structure would result in the increase of band gap. Based on the above analysis, it is reasonable to conclude that both the two factors cause the increase of band gap with increasing annealing temperature.

IV. CONCLUSION

In summary, The effects of postdeposition annealing on the structure and optical properties of YO_xN_y films have been investigated. The XRD result shows that the crystallization starts at the annealing temperature of 500 °C. The surface morphology of YO_xN_y films has been investigated by atomic force microscopy. The result shows that the roughness root mean square (rms) value is increased with the increase of the annealing temperature, which is likely due to crystallization-induced large grain size at higher temperature annealing. The optical properties of YO_xN_y films have been measured by SE. The results show that the optical properties of these films are strongly affected by high temperature annealing. It was found that the refractive index (n) of YO_xN_y films decreased with the increase of annealing temperature

Downloaded 21 Jun 2010 to 61.190.88.137. Redistribution subject to AIP license or copyright; see http://jap.aip.org/jap/copyright.jsp

below 600 °C, whereas it increased with increasing annealing temperature above 600 °C, which is due to the combined effects of the higher packing density and the reduction of N content in YO_xN_y films upon high temperature annealing. The optical band gap of YO_xN_y films was found to increase with the increase of annealing temperature, which is due to the reduction of N content and the crystallization of YO_xN_y films upon high temperature annealing. From the results discussed above, SE is believed to be an effective technique to analytically characterize high-*k* gate dielectrics, a technologically important and challenging class of materials.

ACKNOWLEDGMENTS

This work was supported by National Natural Science Foundation of China (Grant No. 10674138)

[1]G. D. Wilk, R. M. Wallace, and J. M. Anthony, J. Appl. Phys. **89**, 5243 (2001).
[2]K. J. Hubbard and D. G. Schlom, J. Mater. Res. **11**, 2757 (1996).
[3]S. Guha, E. Cartier, M. A. Gribelyuk, N. A. Bojarczuk, and M. C. Copel, Appl. Phys. Lett. **77**, 2710 (2000).
[4]J. Robertson, J. Vac. Sci. Technol. B **18**, 1785 (2000).
[5]J. Kwo, M. Hong, A. R. Kortan, K. T. Queeney, Y. J. Chabal, J. P. Mannaerts, T. Boone, J. J. Krajewski, A. M. Sergent, and J. M. Rosamilia, Appl. Phys. Lett. **77**, 130 (2000).
[6]L. A. Ragnarsson, S. Guha, M. Copel, E. Cartier, N. A. Bojarczuk, and J. Karasinski, Appl. Phys. Lett. **78**, 4169 (2001).
[7]A. I. Kingon, J.-P. Maria, and S. K. Streiffer, Nature (London) **406**, 1032 (2000).
[8]M. Quevedo–Lopez, M. El–Bouanani, S. Addepalli, J. L. Duggan, B. E. Gnade, R. M. Wallace, M. R. Visokay, M. Douglas, and L. Colombo, Appl. Phys. Lett. **79**, 4192 (2001).
[9]M. A. Quevedo–Lopez, M. El–Bouanani, M. J. Kim, B. E. Gnade, R. M. Wallace, M. R. Visokay, A. Li–Fatou, M. J. Bevan, and L. Colombo, Appl. Phys. Lett. **81**, 1609 (2002).
[10]C. S. Kang, H.-J. Cho, K. Onishi, R. Nieh, R. Choi, S. Gopalan, S. Krishnan, J. H. Han, and J. C. Lee, Appl. Phys. Lett. **81**, 2593 (2002).
[11]L. Miotti, C. Driemeier, F. Tatsch, C. Radtke, V. Edon, M. C. Hugon, O. Voldoire, B. Agius, and I. J. R. Baumvol, Electrochem. Solid-State Lett. **9**, F49 (2006).
[12]J. M. Howard, V. Craciun, V. Essary, and R. K. Singh, Appl. Phys. Lett. **81**, 3431 (2002).
[13]S. Jeon, C.-J. Choi, T.-Y. Seong, and H. Hwang, Appl. Phys. Lett. **79**, 245 (2001).
[14]S. Maikap, J.-H. Lee, R. Mahapatra, S. Pal, Y. S. No, W.-K. Choi, S. K. Ray, and D.-Y. Kim, Solid-State Electron. **49**, 524 (2005).
[15]R. P. Vasquez and A. Madhukar, Appl. Phys. Lett. **47**, 998 (1985).
[16]G. V. Soares, K. P. Bastos, R. P. Pezzi, L. Miotti, C. Driemeier, I. J. R. Baumvol, C. Hinkle, and G. Lucovsky, Appl. Phys. Lett. **84**, 4992 (2004).
[17]L. Q. Zhu, L. D. Zhang, G. H. Li, G. He, M. Liu, and Q. Fang, Appl. Phys. Lett. **88**, 232901 (2006).
[18]S. J. Wang, J. W. Chai, Y. F. Dong, Y. P. Feng, N. Sutanto, J. S. Pan, and A. C. H. Huan, Appl. Phys. Lett. **88**, 192103 (2006).
[19]S. Toyoda, J. Okabayashi, H. Takahashi, M. Oshima, D. I. Lee, S. Sun, S. Sun, P. A. Pianetta, T. Ando, and S. Fukuda, Appl. Phys. Lett. **87**, 182908 (2005).
[20]N. V. Nguyen, C. A. Richter, Y. J. Cho, G. B. Alers, and L. A. Stirling, Appl. Phys. Lett. **77**, 3012 (2000).
[21]X. Wang and P. J. Martin, Appl. Phys. Lett. **68**, 1177 (1996).
[22]P. Scherrer, Nachr. Ges. Wiss. Goettingen, Math.-Phys. Kl. **2** 98 (1918).
[23]M.-H. Cho, D.-H. Ko, K. Jeong, S. W. Whangbo, C. N. Whang, S. C. Choi, and S. J. Cho, Thin Solid Films **349** 266 (1999).
[24]J. F. Moulder, W. F. Stickle, P. E. Sobol, and K. D. Bomben, *Handbook of X-ray Photoelectron Spectroscopy* (Perkin-Elmer Corporation, Eden Prairie, MN, 1992).
[25]G. E. Jellison and F. A. Modine, Appl. Phys. Lett. **69**, 371 (1996); **69**, 2137 (1996).
[26]D. E. Aspnes, J. B. Theeten, and F. Hottier, Phys. Rev. B **20**, 3292 (1979).
[27]Z. Song, B. R. Rogers, and N. D. Theodore, J. Vac. Sci. Technol. A **22**, 711 (2004).
[28]M. Ohring, *The Materials Science of Thin Films* (Academy, San Diego, CA, 1991).
[29]H. Hu, C. X. Zhu, Y. F. Lu, T. Liew, M. F. Li, B. J. Cho, W. K. Chio, and N. Yakovlev, J. Appl. Phys. **94**, 551 (2003).
[30]N. V. Nguyen, S. Sayan, I. Levin, J. R. Ehrstein, I. J. R. Baumvol, C. Driemeier, C. Krug, L. Wielunski, P. Y. Hung, and A. Diebold, J. Vac. Sci. Technol. A **23**, 1706 (2005).
[31]G. Shang, P. W. Peacock, and J. Robertson, Appl. Phys. Lett. **84**, 106 (2004).
[32]S. Sayan, N. V. Nguyen, J. Ehrstein, T. Emge, E. Garfunkel, M. Croft, X. Zhao, D. Vanderbilt, I. Levin, E. P. Gusev, H. Kim, and P. J. McIntyre, Appl. Phys. Lett. **86**, 152902 (2005).

Downloaded 21 Jun 2010 to 61.190.88.137. Redistribution subject to AIP license or copyright; see http://jap.aip.org/jap/copyright.jsp